JOURNAL OF GEOPHYSICAL RESEARCH, VOL. 101, NO. C2, PAGES 3509–3524, FEBRUARY 15, 1996

Near-inertial oscillations over the Texas-Louisiana shelf

Changsheng Chen
Department of Marine Sciences, University of Georgia, Athens

Robert O. Reid and Worth D. Nowlin Jr.
Department of Oceanography, Texas A&M University, College Station

Abstract. Wind-induced, near-inertial oscillations over the Texas-Louisiana shelf in spring and summer 1992 are described using the current and wind observations taken during the first year of the Texas-Louisiana Shelf Circulation and Transport Processes Study (LATEX A). Rotary spectral analysis shows clockwise-rotating energy peaks at near-inertial frequencies for records from all current meter moorings after the suppression of principal tidal signals. The vertical structure of near-inertial oscillations is characterized by a first baroclinic mode with a near 180° phase difference between the upper mixed layer and the lower stratified layer. The oscillations are intermittent with a modulation timescale of about 5–10 days. They are surface-intensified and have maximum values near the shelf break, decaying gradually toward the coast but rapidly offshore. Near-inertial oscillations appear to accompany a sudden change of the wind stress during frontal passages. Diagnostic analysis suggests that the large near-inertial oscillations over the LATEX shelf are mainly generated by high-frequency (near-inertial) variation of the wind stress accompanying the passage of atmospheric fronts. When the downward transfer of the near-inertial energy to the deep stratified layer is small, a simple mixed layer model forced by the observed wind stress provides a reasonable prediction of the near-inertial currents in the mixed layer.

1. Introduction

Near-inertial oscillations are known to exist widely within the ocean. They are seen as clockwise (counterclockwise) rotating, near-circular horizontal currents in the northern (southern) hemisphere, with frequencies slightly greater than the local inertial frequency [*Webster*, 1968; *Munk and Phillips*, 1968]. Many observational and theoretical studies suggest that the near-inertial motion can be generated by sudden changes of the surface wind stress associated with the local wind field [*Ekman*, 1905; *Pollard*, 1970; *Kundu and Thompson*, 1985], passage of a hurricane [*Brooks*, 1983; *Price*, 1983; *Gill*, 1984], and sea breeze [*Barron and Vastano*, 1994]. Inertial motions also can be initiated when tidal energy is transferred into low-frequency baroclinic gravity waves by the interaction of the barotropic tide with bottom topography [*Hendershott*, 1973].

The temporal and spatial structures of near-inertial oscillations vary with forcing and location. In the open ocean, wind-induced, near-inertial motion is mainly characterized by the local wind field, thickness of the mixed layer, and vertical stratification. The oscillations are observed to be intensified near the surface and are reduced as the mixed layer deepens [*Gill*, 1982]. They are intermittent with typical modulation scales of 5–7 days and horizontal coherence scales of 20–60 km [*Munk and Phillips*, 1968; *Fu*, 1981; *Nowlin et al.*, 1986]. Although these oscillations are most energetic in the mixed layer, inertial energy can propagate downward to the deep ocean through the main thermocline, leading the deep water to oscillate [*Kroll*, 1975; *Nowlin et al.*, 1986]. In the coastal region, however, the amplitude and spatial structure of near-inertial oscillations are constrained by the coastline and modified due to the bottom topography. Amplitudes of the oscillations must decrease toward the coast to match the boundary condition of no flow across the coastline.

Long shelf waves with subinertial frequencies are trapped near the coast and decay offshelf [*Clarke and Brink*, 1985]. The character of inertial waves may be modified due to coupling with coastal shelf waves over the shelf. At latitudes where the local inertial frequency is close to principal tidal frequencies, the inertial oscillations can be affected not only by the temporal variation of surface wind stress but also by the energy transfer from tidal motions when the barotropic tide interacts with the slope [*Hendershott*, 1973].

As a major observational component of the Texas-Louisiana Shelf Circulation and Transport Study (LATEX A program), an array of moored current meters and meteorological buoys was deployed in April 1992, to make 3-year measurements of circulation and near-surface wind field over the LATEX shelf. Mooring locations are shown in Figure 1. Principal objectives of this program are to study the seasonal and interannual variability of low-frequency currents over the LATEX shelf and associated dynamical processes. This program is ongoing; we focus attention here on an examination of near-inertial and tidal motions over the shelf, based on observations from the spring and summer of 1992.

Brooks [1983] found strong near-inertial oscillations with amplitudes reaching 50 cm/s and durations of 8 days over the western Texas slope following the passage of Hurricane Allen in the summer of 1980. These oscillations were coherent at 100-km horizontal and 500-m vertical separations. Satellite-tracked, near-surface drifter measurements carried out over the LATEX shelf in the spring of 1989 [*Barron and Vastano*,

Paper number 95JC03395.
0148-0227/96/95JC-03395$05.00

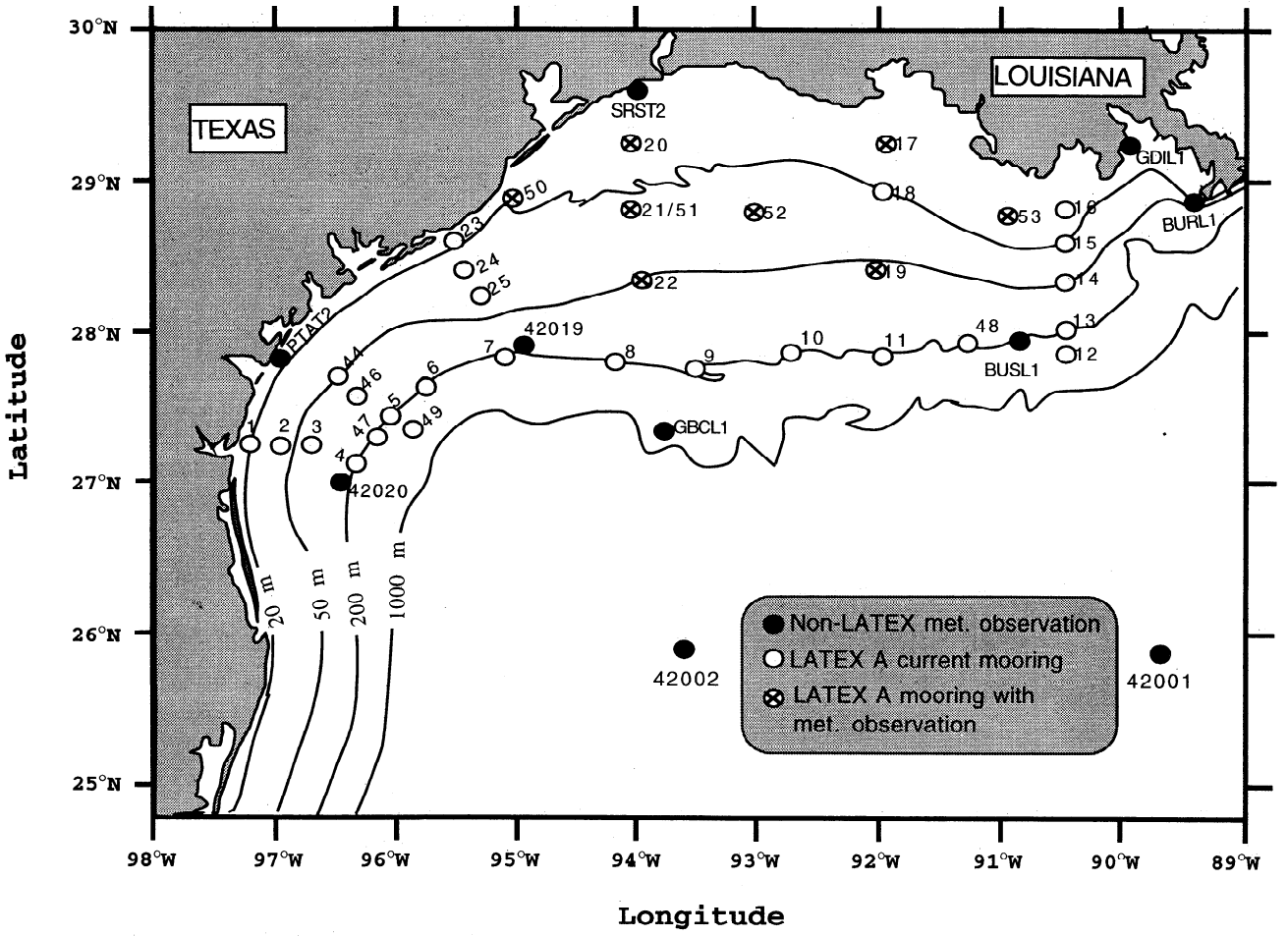

Figure 1. Locations of current meter moorings and meteorological buoys from which data are used in this study. The LATEX A meteorological buoys are located at moorings 17, 19, 20, 21/51, 22, 50, 51, and 53. Non-LATEX meteorological observations are indicated by solid circles.

1994; *Vastano and Barron*, 1994] show strong inertial oscillations with amplitudes of 21 and 54 cm/s near the shelf break. Previous observations provide good examples of near-inertial oscillations over the Texas slope. Little has been reported, however, regarding the structures of near-inertial motions generated by the local wind field over the LATEX shelf.

The LATEX shelf is bounded to the north and northwest by the coast. The range of latitude from the coast to the continental slope (east of 96°W where shelf current meter moorings are located) is from about 29.5°N to 27.0°N. Thus the local inertial periods over this shelf range from 24.3 to 26.3 hours close to the K_1 tidal period (23.9 hours) in the north and the O_1 tidal period (25.8 hours) in the south. Since inertial and diurnal tidal frequencies are so close in this region, the removal of tidal motions from observed current records becomes our first task in the study of wind-induced, near-inertial oscillations.

A strong sea breeze occurs in the coastal region of the LATEX shelf, particularly in summer when the diurnal variation of cross-shelf gradient of air temperature is large [*Hsu*, 1972]. The local sea breeze plus a sudden change in the synoptic wind field may cause large near-inertial motions near the coast. Examining the cross-shelf scale of the sea breeze is of importance in determining the driving mechanism of near-inertial oscillations over the shelf.

The general geometry of the LATEX shelf is one of isobaths almost parallel to the coast (see Figure 1). The water depth gradually increases offshore to approximate 70 m, beyond which it deepens somewhat more steeply to 200 m at the shelf break. Farther offshore, depth sharply deepens to 1000 m within a few kilometers on the break. This bathymetric configuration is not only favorable for the generation of coastal shelf waves and forced internal tides on the slope but also affects the cross-shelf structure of near-inertial oscillations.

This paper consists of nine sections. The database is described in section 2. The rotary spectra for 3-hour, low-passed currents are estimated and discussed in section 3. Section 4 gives results of the harmonic analysis for the principal tidal currents and the suppression of such tides from our records. Section 5 shows the spatial structure of near-inertial oscillations based on band-passed currents at local inertial frequencies. Measurements of the wind field are described in section 6. In section 7 the driving mechanisms of near-inertial oscillations are discussed based on a simple slab-like mixed layer model. A driving mechanism for the observed near-diurnal variation of surface wind stress over the entire shelf is proposed in section 8. Finally, a summary is given in section 9.

2. The Data

Five types of current meters (Endeco 174 SSM and DMT, Aanderaa RCM 4/5 and 7/8, and InterOcean S4) were de-

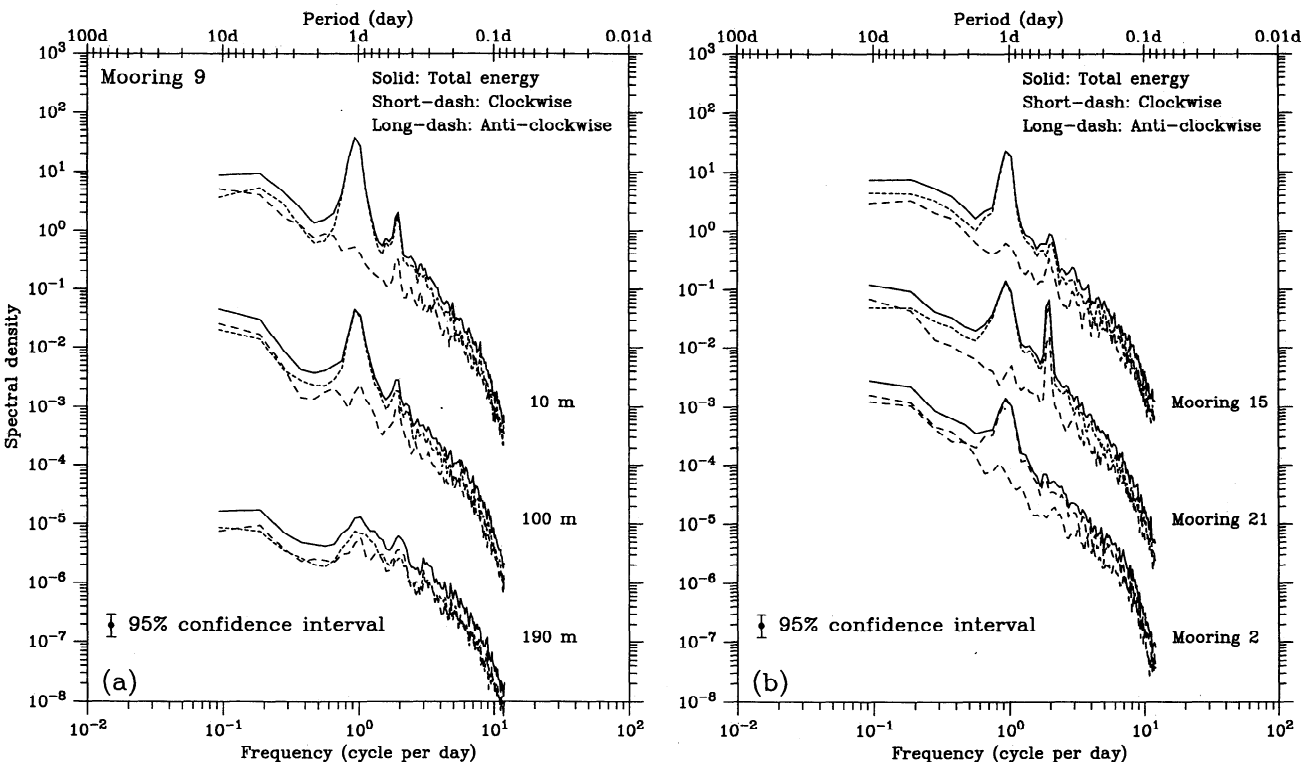

Figure 2. Rotary spectra of current records from (a) depths of 10, 100, and 190 m at mooring 9 and (b) 10 to 12-m instruments on moorings 15, 21, and 2. See Figure 1 for locations. The spectra at 100 m in Figure 2a and mooring 21 in Figure 2b are shifted downward by 10^2, and spectra at 190 m in Figure 2a and mooring 2 in Figure 2b are shifted by 10^4. Estimates of rotary spectra were made using the 3-hour, low-passed data sampled hourly from April 15 to July 22, 1992. Segment points of 256 with overlap points of 128 were used for spectral analysis. Spectral density is in $(cm/s)^2/cpd$.

ployed in the LATEX A array pictured in Figure 1. Instruments were placed at three nominal depths of 10–12, 100, and 190 m on moorings located on the outer shelf and at depths of 10–12 m and near bottom on moorings located in less than 100-m water depth.

Meteorological parameters were measured simultaneously from coastal stations, oil platforms, NOAA buoys in the central Gulf, and eight LATEX A meteorological buoys located at moorings 17, 19, 20, 21/51, 22, 50, 52, and 53 (Figure 1). Horizontal wind velocity, barometric pressure, and air and sea surface temperatures were recorded hourly. LATEX A oceanic and atmospheric data collection began in mid-April 1992 for a period of about 30 months. The analysis carried out in this study is limited to the first 8 months of data.

Speed and direction of horizontal currents, water temperature, and salinity were recorded at 5- or 30-min intervals on most of current meters. For this analysis, records were joined end to end over time to construct longer time series. Gaps of less than 4 hours were linked by linear interpolation; longer gaps were not bridged. Each joined time series was filtered using a 3-h, low-passed Lanczos filter, and then resampled hourly. The 40-hour, low- and high-passed data were obtained by repeating the low-passed Lanczos filter using a 81-point, symmetric weight with half-power point at 40 hours. The 40-hour, high-passed current meter records were at 1-hour resolution but the 40-hour, low-passed data were subsampled at 6-hour intervals. Time series of surface wind, air pressure, and air and water temperatures were treated likewise.

3. General Energy Spectra

Rotary spectra are widely used to analyze time series of current vector fields [*Gonella*, 1972; *Mooers*, 1973; *Denbo and Allen*, 1984]. Because spectra for clockwise- and counterclockwise-rotating motions can be separately expressed, rotary spectral estimates, in general, are useful in identifying near-inertial motions that have circular anticyclonic rotation. Over the LATEX shelf, however, both diurnal tidal and inertial motions are clockwise-rotating and close in frequency, and thus it is difficult to separate one from the other by this method. The rotary spectra presented here contain the energy for both tidal and inertial motions.

Rotary spectra were obtained from all of the 3-hour, low-passed current records during the study period of April–October 1992. Distributions of rotary spectral energy were quite similar over the entire shelf. Figure 2 shows examples at depths of 10, 100, and 190 m from mooring 9 on the 200-m isobath at the shelf break and at 10–12 m on moorings 15, 21, and 2, located from east to west near the 20-m isobath. A prominent spectral peak centered at near-diurnal frequency was found at all levels, and the amplitudes decreased with increasing depth. The energy contributing to this near-diurnal peak was essentially all clockwise-rotating motion near the surface and middepth, with somewhat larger contributions from counterclockwise rotation near the bottom.

A principally clockwise-rotating spectral peak was also found at semidiurnal frequencies over the shelf. The ampli-

tudes were largest in the nearshore portion of the central LATEX shelf and decreased significantly offshore and toward both eastern and southwestern portions of this shelf. The semidiurnal peak is believed to represent the energy of semidiurnal tidal currents. This spatial distribution of the semidiurnal energy over the shelf is in agreement with a simple theory of tidal waves proposed by *Clarke* [1991]. According to that work, at latitudes where tidal frequencies are higher than the local inertial frequency, the interaction of barotropic tides with the continental shelf leads to large amplification of semidiurnal tides across wider continental shelves, while amplitudes generally decrease away from the coastal zone.

4. Suppression of Principal Tidal Currents

Previous observations of sea surface elevation near the coast show that the most significant tidal constituents in the LATEX shelf region are two diurnal (K_1 and O_1) and three semidiurnal (M_2, N_2, and S_2) tides [*Reid and Whitaker*, 1981]. Periods of K_1 and O_1 are 23.9 and 25.8 hours, while local inertial periods range from 24.3 hours at 29.5° on the northern shelf to 25.7 hours at 27.8° near the shelf break. Because local inertial periods are so close to K_1 tidal period near the coast and O_1 tidal period near the shelf break, their separation using a frequency band filter is difficult.

On the other hand, tidal and inertial motions result from different physical processes and they have no long-term coherence. Wind-induced, near-inertial oscillations, in general, are intermittent with modulation timescales of only a few days. Based on Rayleigh criterion, therefore, it is possible to remove most of the near-inertial energy from diurnal tidal currents by harmonic analysis if the time series of the currents is long enough.

An updated harmonic analysis program developed originally by *Foreman* [1979] was used to estimate amplitudes and phases of the five tidal constituents: K_1 and O_1, M_2, N_2, and S_2. It is a least squares fitting program with modification from nodal modulation and astronomical argument correction. Unlike previous harmonic analysis methods, this program has no restriction for particular record length and can be used for current data with gaps. Some tests were made to examine the effect of record length on the resulting amplitudes of diurnal tidal currents. An example is shown in Table 1 for the 12-m records from mooring 13 on the 200-m isobath. The local inertial period at this mooring is 25.4 hours, which is close to the O_1 tidal period. The estimated amplitude of the O_1 tidal current was dramatically increased when a strong inertial event was included in the analysis for a 3-month time series (compare case A with case B in Table 1). Thereafter, the contributing effects of local inertial motions to the diurnal tidal current estimates decreased as the record length increased, even though several additional inertial events were included. The estimated phases of diurnal tidal currents showed greater sensitivity to the record length. This suggests that there still was some near-inertial energy in diurnal tidal currents estimated by the least squares harmonic analysis, even for long records. Because estimated amplitudes tend to be close as the record length increased, we believe here that most of near-inertial energy has been removed from tidal currents in the least squares harmonic analysis for a long time series. Based on this argument, we used all available current meter records (starting in mid-April 1992 to early January 1993; about 8 months) to estimate tidal currents with the harmonic analysis method.

Table 1. Comparison of the Tidal Current Amplitude at 12 m on Mooring 13

	U, cm/s		*V*, cm/s	
Case	O_1	K_1	O_1	K_1
A	3.1	2.8	3.3	1.3
B	6.8	3.7	6.8	3.1
C	3.2	3.2	3.5	3.1
D	2.4	3.1	2.4	2.6

Case A, estimated on the basis of 2-month records from April 17 through June 30, 1992; case B, estimated on the basis of 3-month records from April 17 through July 22, 1992, in which strong inertial oscillations occurred in mid-July; case C, estimated on the basis of 6-month records from April 17 through October 20, 1992; case D, estimated on the basis of 8-month records from April 17, 1992 through January 10, 1993.

Comparisons of the total kinetic energy spectra for the 3-hour low-passed records (containing the tidal signal) and residual records (estimated tidal signal removed) were made for all current meters on each LATEX A mooring. Examples are shown in Figure 3 at 10, 100, and 190 m on mooring 9 at the shelf break and at 10–12 m on moorings 15, 21, and 2, located from east to west along the 20-m isobath. For cases with a strong semidiurnal peak like mooring 21, the removal of the tidal energy greatly suppresses the semidiurnal peak, while cases with weak semidiurnal peaks seem unchanged at the 95% confidence level after removal of the estimated tide. This could be attributed to the fact that the tidal suppression is carried out by subtracting the estimated tidal signal from the raw record and errors in phase associated with weak tidal signal can cause the residual record to show little changes in its variance spectrum.

Removal of the K_1 and O_1 tidal signals at each current meter, while of comparable energy to that of the largest M_2 tidal signal, has little effect on the near-inertial spectral peaks in the residual spectra except for those near the coast. In general, the internal tides are intensified near the bottom of the slope where the interaction of barotropic tide and bottom topography is strongest. However, the diurnal oscillations (a sum of barotropic tides, internal tides, and near-inertial oscillations) were found very weak at the LATEX bottom current meters at shelf break. Because of that, we have not taken the internal tides into accounts in our present work.

5. Spatial Distribution of Near-Inertial Currents

Here we describe the spatial distribution of near-inertial currents observed over the LATEX shelf in spring and summer, 1992, prior to the occurrence of Hurricane Andrew. In this study, we characterize near-inertial motions as the band-passed, residual currents filtered by a digital, nonphase distorted filter with a band width of admitting periods from 22 to 28 hours. The band width was selected to include all inertial periods ranging from 24.3 hours on the northern shelf near the coast to 26.2 hours on the southern edge of the shelf near 27°N. Some tests, using a varying band width centered at the local inertial frequency for different moorings, were made to examine the effects of frequency band width on the resulting band-passed currents. Because high-frequency (40-hour high passed) signals at each LATEX A mooring were dominated by

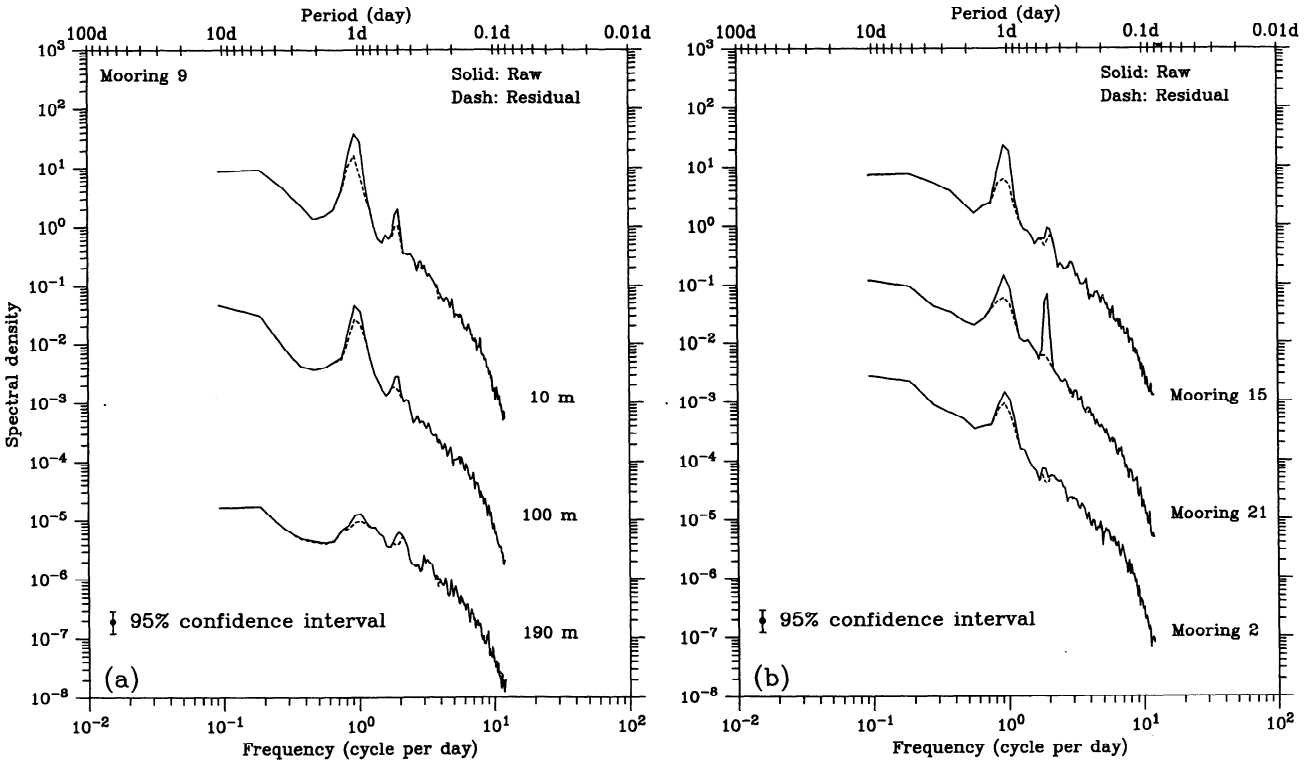

Figure 3. Rotary spectra of clockwise components of raw (with tide) and residual (tide suppressed) currents at (a) depths of 10, 100, and 190 m on mooring 9 and (b) 10–12 m on moorings 15, 21, and 2. The spectra at 100 m in Figure 3a and mooring 21 in Figure 3b are shifted downward by 10^2; those from 190 m in Figure 3a and mooring 2 in Figure 3b by 10^4. Estimates and units are as described in Figure 2.

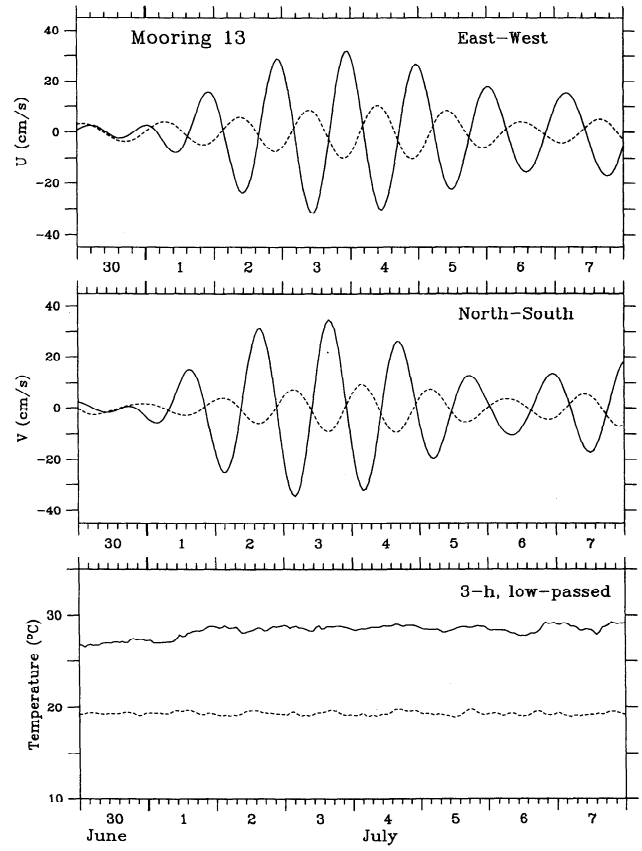

Figure 4. Time series of the band-passed, residual currents and the 3-hour, low-passed water temperature from June 30 to July 7, 1992, at depths of 12 m (solid line) and 100 m (dashed line) on mooring 13. The width of the frequency band is from 1/(28 hours) to 1/(22 hours).

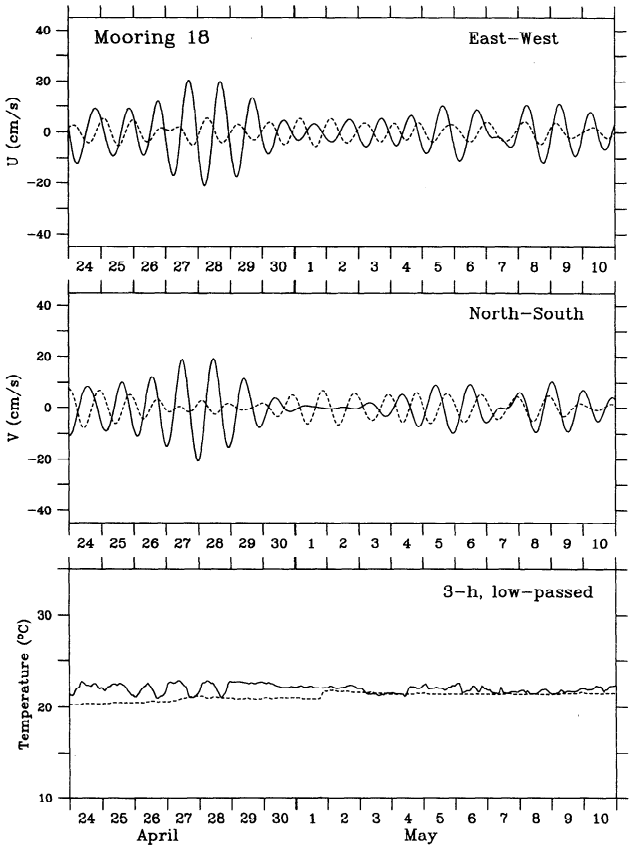

Figure 5. Time series of the band-passed, residual currents and the 3-hour, low-passed water temperature from April 24 to May 10, 1992, at depths of 10 m (solid line) and 19 m (dashed line) on mooring 18. The frequency band width is from 1/(28 hours) to 1/(22 hours).

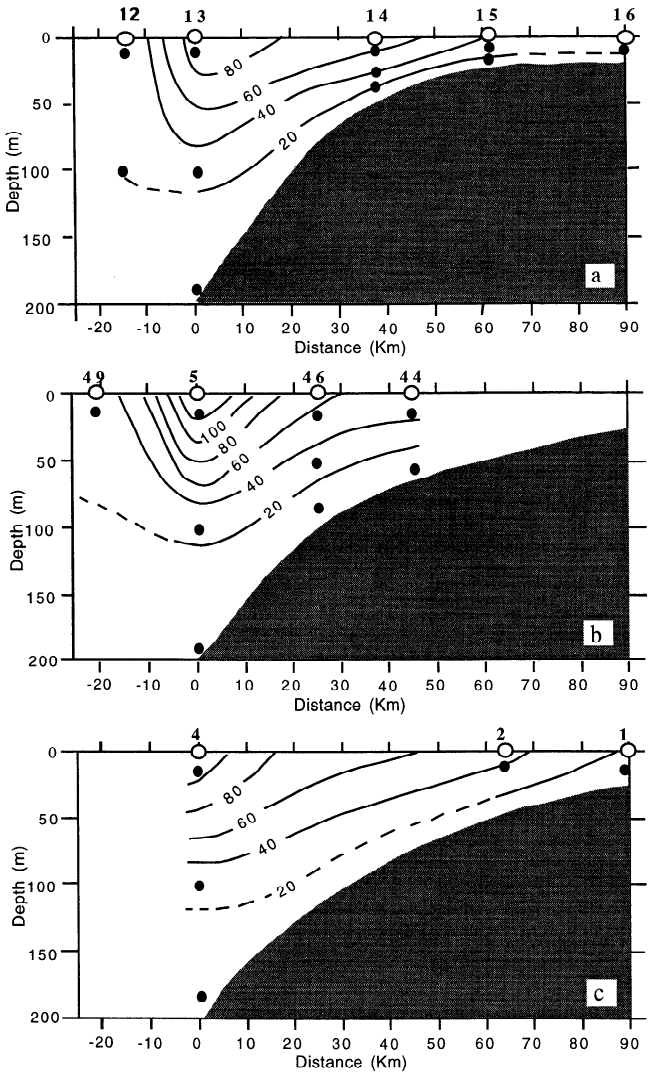

Figure 6. Distributions of the variance of the band-passed, residual currents observed from April 15 to July 22, 1992, at three cross-shelf sections over the LATEX shelf. See Figure 1 for locations. Mooring numbers are shown above each section. The contour units are cm^2/s^2.

the near-inertial motions, and the inertial energy was concentrated in a relatively narrow band near the local inertial frequency, few differences were found in the resulting band-passed currents.

Vertical structures. In general, the amplitude of near-inertial currents decreased with depth at each mooring over the entire shelf. For example, at mooring 13 the maximum amplitude of oscillating currents during a strong near-inertial event in early July was near 30 cm/s at 12 m but decreased with depth to about 10 cm/s at 100 m (Figure 4).

Vertical phase distribution of near-inertial currents was characterized by a first-baroclinic mode-like structure in mixed and stratified layers. An example is shown in Figure 4 for mooring 13 where near-inertial oscillations at 100 m were about 180° out of phase with those at 10 m at the time of the strong oscillation event in the early July. The mixed-layer depth was about 12 m during that event, and the temperature contrast between the two instruments was large. The resulting vertical structure of oscillations was similar to that of a two-layer system. This vertical structure is very similar to that reported by *Millot and Crepon* [1981] on the continental shelf of the Gulf of Lions and by T. M. Wood and D. Chapman (unpublished manuscript, 1987) at Nantucket Shoal over the New England shelf.

Such vertical structure in velocity tends to disappear when the vertical density stratification weakens. An example is seen at mooring 18 (Figure 5). The near-inertial oscillations there were strong from the beginning of the record until April 30 and again starting about May 5. Even though the thermal and density contrasts between the 10-m and 19-m instruments were never large, there was distinct vertical stratification during the first significant inertial oscillations, and hence the oscillations at the two levels were nearly out of phase. As the stratification effectively disappeared during the latter part of the records, the oscillations in the two layers became nearly in phase.

The opposing phases found in mixed and stratified layers can be explained using a simple two-layer model. On assumption of a rigid lid, the cross-shelf mass flux in the vertical must vanish because of the no-flux boundary condition at coast. This means that the cross-shelf transport in the upper layer must be equal in magnitude and opposite in phase to that in the lower layer. The ratio of the current speed in the upper layer to that in the lower layer is inversely proportional to the thickness of upper mixed layer, decreasing as the mixed layer becomes deeper.

Horizontal structures. The cross-shelf differences of near-inertial energy are clearly seen in the cross-shelf distributions of the variance calculated for band-passed, near-inertial current records from mid-April to late July 1992. Examples are shown in Figure 6 for three cross-shelf sections of current measurements. Figure 6 also summarizes the vertical structure of near-inertial oscillations.

The variance of near-inertial motions is maximum near the shelf break at all measured locations on the LATEX shelf and decays gradually onshore but rapidly offshore. The maximum values of variance were about 100 cm^2/s^2 (at 10 m) at the shelf break, while the near-surface (10 m) values over the inner shelf were about 20 cm^2/s^2.

Along-shelf distribution of near-inertial energy on the 200-m isobath was complex. The variance estimated by the band-passed current records from mid-April to late July (Figure 7)

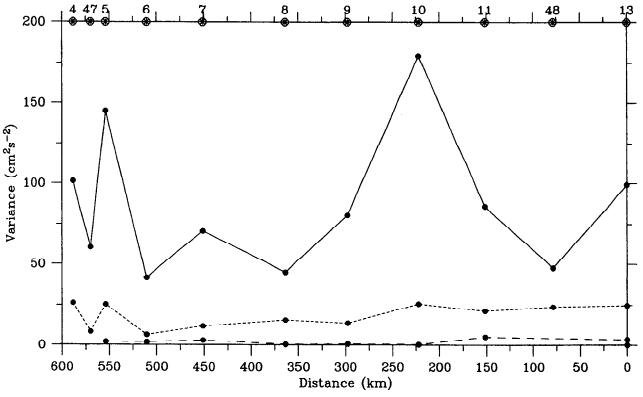

Figure 7. Distributions of the variance of the band-passed, residual currents observed from April 15 to July 22, 1992, along the 200-m isobath from east to west. Solid, short-dashed, and long-dashed lines refer to variances at 10–12 m, 100 m, and 190 m moorings. Mooring numbers are shown at the top of the figure. The contour units are cm^2/s^2.

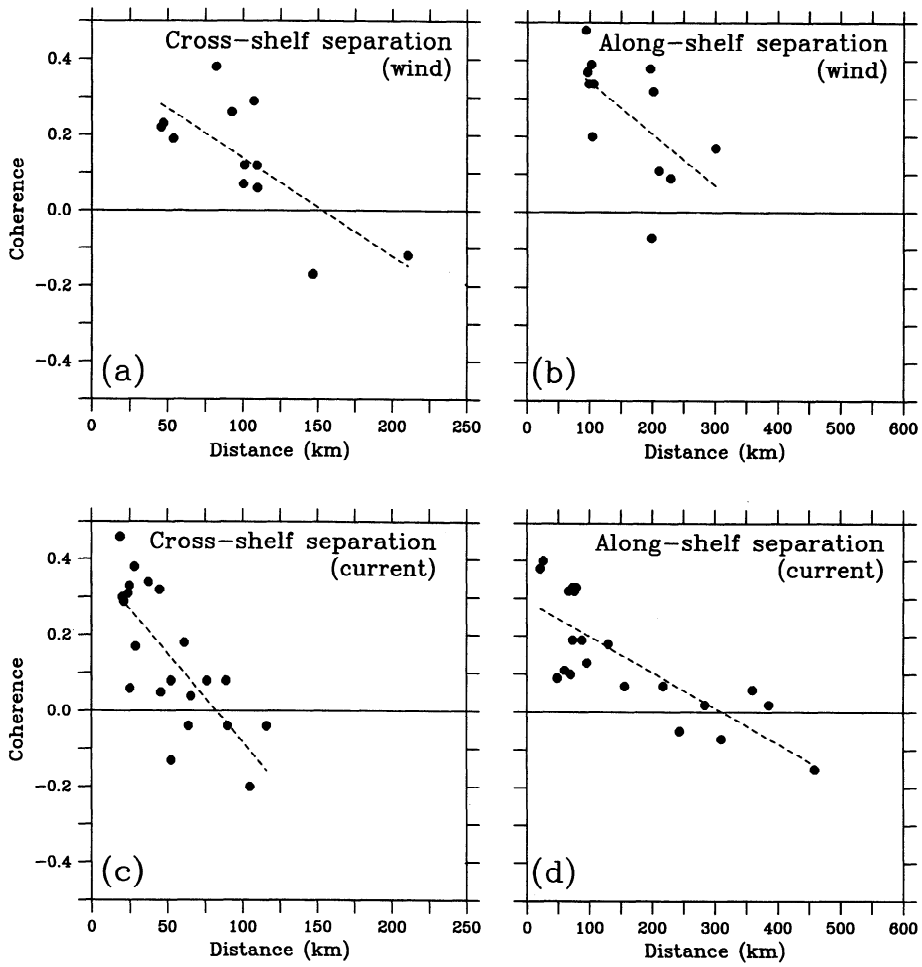

Figure 8. Coherences of the wind (at diurnal frequency) and the residual current (at near-inertial frequencies) relative to the 95% confidence level for (a and c) cross-shelf and (b and d) along-shelf stations pairs over the LATEX shelf. Estimates for both wind and current were made using the hourly sampled data from April 15 to July 22, 1992. Each solid circle indicates the coherence value for an individual pair, and the dashed line represents the least squares fit for all points. See text for full explanation of procedure.

shows rather low, near-surface energy levels at moorings 48, 8, 6, and 47 and highs at moorings 10 and 5. Few differences were observed in the along-shelf direction for the energy levels of deeper near-inertial oscillations.

Coherences of near-inertial oscillations were estimated for cross-shelf and along-shelf separations using residual current records from the upper (10–12 m) instruments. Cross-shelf separations consist of pairs of moorings on every cross-shelf section. Along-shelf separations consist of pairs of moorings along approximately the same isobath. The simultaneous record pairs for the period April to July 1992 were used to compute coherences for both along-shelf current component pairs and cross-shelf current component pairs. The 95% confidence level was subtracted from each coherence, and the coherences for along-shelf components and cross-shelf components were averaged. The resulting averaged relative coherences for near-inertial oscillations were plotted as functions of cross-shelf and along-shelf separations in Figures 8c and 8d. The same record length is used to estimate the coherence for water currents. The 95% confidence value for each pair is 0.43. To compare with coherences of wind stress estimated using different record lengths, we plot the current coherence relative to its 95% confidence level.

The cross-shelf coherence scale of near-inertial oscillations is seen to be about 80 km with regard to a 95% confidence limit (Figure 8c). Individual oscillation events gave quite the same order of separation scale in the cross-shelf direction. An example is shown in Figure 9 for the strong near-inertial event occurring in early July. The oscillations were of almost the same phase from mooring 15 to mooring 13 over a distance of about 80 km, while offshore of mooring 13 the oscillations are distinctly different.

Relative to the 95% confidence levels, the along-shelf coherence scale of near-inertial motions can be estimated as 300–350 km (Figure 8d), about 4 times as large as for cross-shelf separations. The along-shelf separation scale for an individual event can be seen in Figure 10. The oscillations in late June and early July appeared coherent in both amplitude and phase along the shelf for moorings 13–8 over a distance of about 350 km, but there was little phase agreement for moorings 7–4 in the region where isobaths curve to a more SW-NE orientation.

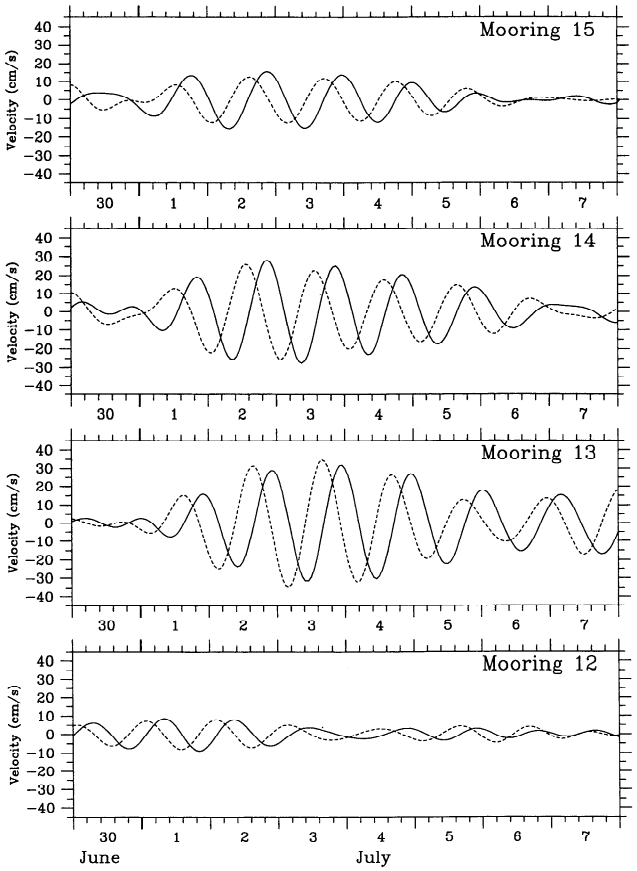

Figure 9. Time series of the band-passed, residual currents at top meters of moorings 15, 14, 13, and 12 during June 30 to July 7, 1992. Solid and dashed lines are the east-west (u) and south-north velocity (v) components, respectively. The frequency band width is from 1/(28 hours) to 1/(22 hours).

6. Meteorological Field

Generally speaking, the near-surface atmospheric flow over the LATEX shelf in spring and summer of 1992 was dominated by a subtropic anticyclone with high pressure centered near 27°N east of Florida. This large-scale high-pressure system produced a southeast, or sometimes south, wind at the marine boundary layer over the entire shelf. The synoptic-scale wind field was intermittently altered with the passage of fronts associated with low-pressure cells. From late April to May, there were two sudden, significant shifts in the direction of the wind vector as cold fronts swept from the northwest to southeast over the LATEX shelf (Figure 11). The wind stress is calculated based on the neutral, steady-state drag coefficient developed by *Large and Pond* [1981].

A typical example of a frontal passage is shown in Figure 12. The wind direction turned to northerly after the cold front attacked the LATEX shelf on May 4 and reversed to southerly on May 9 as the influence of the subtropical high-pressure cell was reestablished over the shelf after the front passed. In June–July these southeast moving fronts were restricted to north of the LATEX coast due to the seasonal northward shift of the subtropic high-pressure cell. As a result, the air flow was dominated by southeast or southwest wind over the shelf, though two brief periods of northerly wind occurred during frontal passages (Figure 11).

Rotary spectra for hourly wind velocities at all meteorolog-

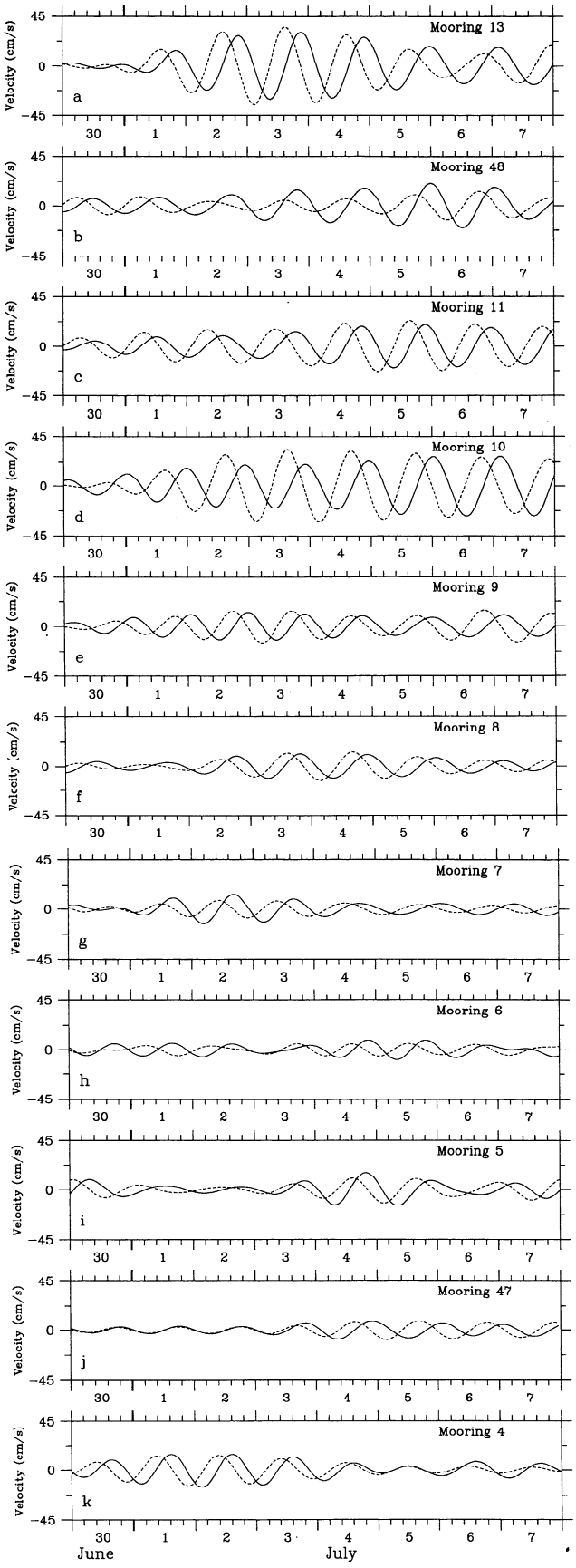

Figure 10. Time series of the band-passed, residual currents at top meters of moorings along the 200-m isobath from east to west during June 30 to July 7. Solid and dashed lines are the along- and cross-shelf components, respectively. The frequency band width is from 1/(28 hours) to 1/(22 hours).

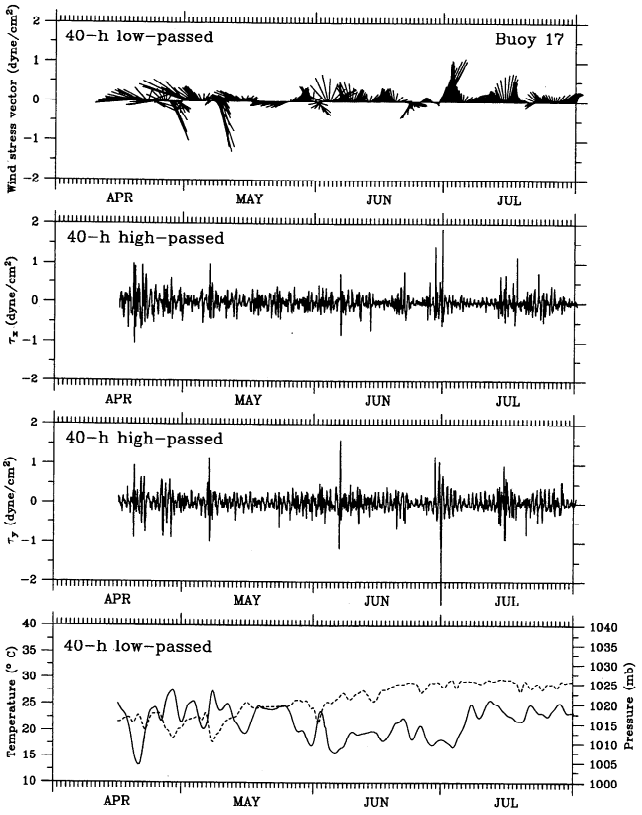

Figure 11. Time series plots for 40-hour, low-passed surface wind stress vectors, 40-hour, high-passed the eastward (x) and northward (y) components of the surface wind stress, and 40-hour, low-passed air temperature (solid line) and pressure (dashed line) at buoy 17 from April through July 1992.

ical buoys over the shelf and in the center of the gulf show a significant peak in clockwise-rotating energy near diurnal period. Figure 13 shows examples of clockwise-rotating energy spectra from locations oriented cross-shelf near 94°W (Figure 1): coastal station SRTS2, LATEX buoys 20–22, and NOAA buoy 42002. The first and second harmonics at 2.0 and 3.0 cpd are also seen in the rotary wind spectra, suggesting that diurnal wind variation was asymmetrically distributed with time over

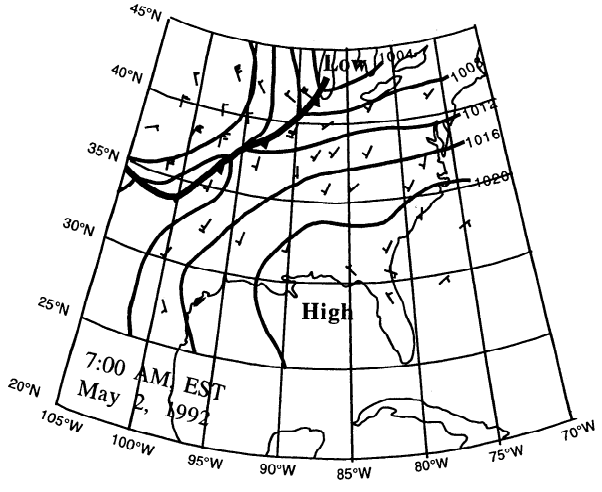

Figure 12. The 1000-mbar weather maps at 0700 LT (7:00 A.M. EST) on May 2, 4, 7, and 9, 1992.

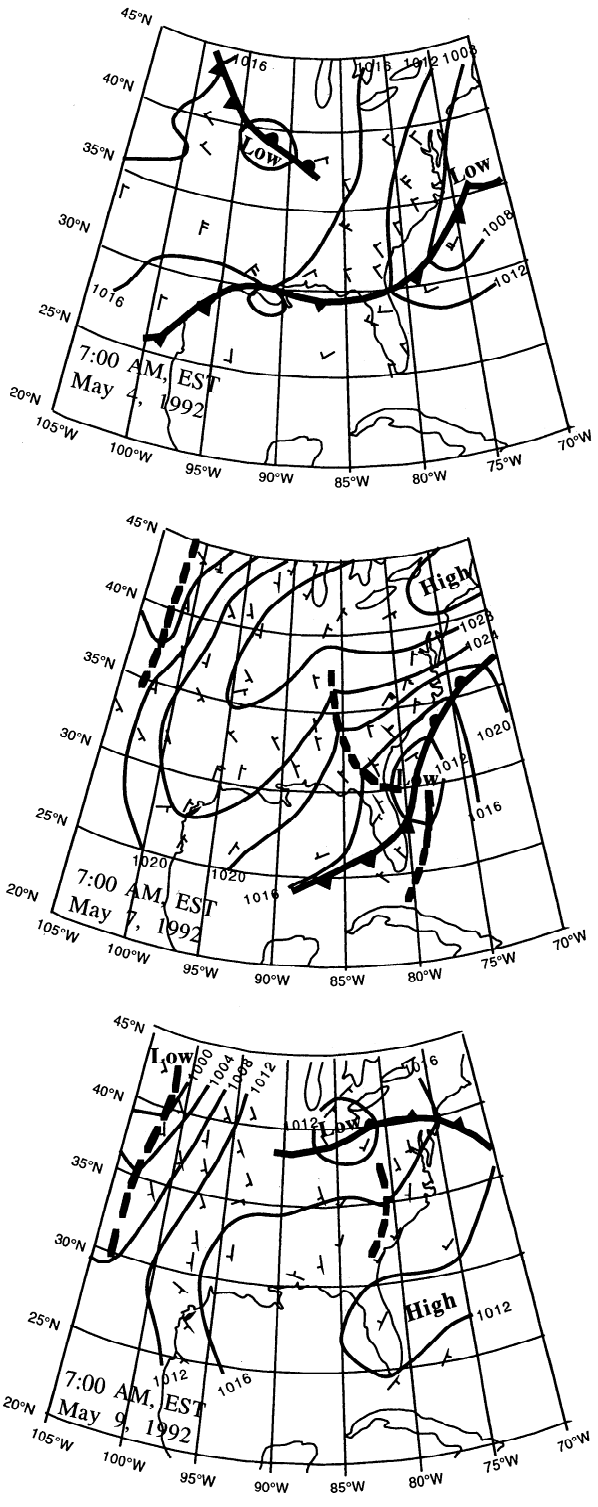

Figure 12. (continued)

the shelf [*Beardsley et al.*, 1987]. The magnitude of the clockwise-rotating diurnal wind energy remained little changed along this section, though some offshore decrease is noted. The peak value of the clockwise energy was 0.32 $(m/s)^2$/cpd at LATEX buoy 22 and 0.19 $(m/s)^2$/cpd at NOAA buoy 42002 located some 375 km south. Large high-frequency wind oscillations appeared to accompany the sudden change of wind vectors during frontal passages (Figure 11).

To examine better the temporal and spatial structures of

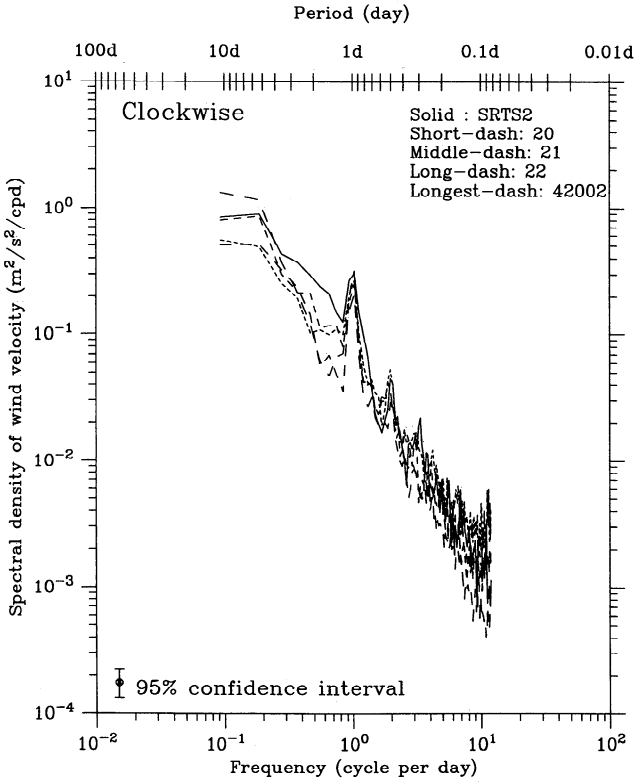

Figure 13. Clockwise-rotating rotary spectra for surface winds at SRST2, LATEX A buoys 20–22, and NOAA buoy 42002. See Figure 1 for locations. Estimates of rotary spectra were made using the hourly sampled wind data obtained from mid-April through late July 1992. Segment points of 256 with overlap points of 128 were used for analysis. Spectral density is in $(m/s)^2/cpd$.

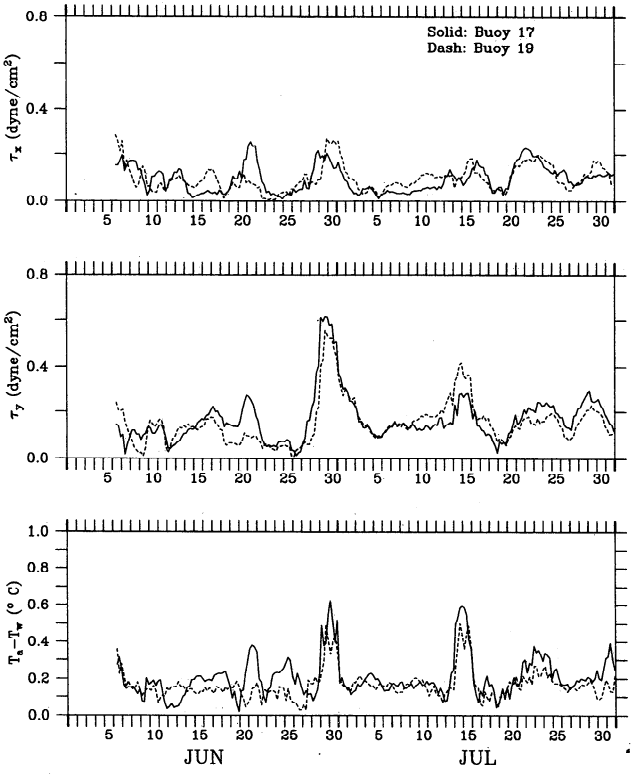

Figure 14. Time series of the eastward (x) and northward (y) surface wind stress components and the air-sea temperature difference at diurnal period calculated by the complex demodulation of data from LATEX A buoys 17 and 19, located on the inner and mid shelf, respectively, near 92°W. A least squares method was used to fit 48-hour segments with a 6-hour overlap.

diurnal wind variation, a complex demodulation at the diurnal period was performed on components of the 40-hour high-passed surface wind stress, the air-sea temperature difference, and surface air pressure using a least squares fit with 48-hour segments and a 6-hour overlap. Figures 14 and 15 illustrate time series of modulated amplitudes of diurnal components of the surface wind stress at two stations oriented across the shelf (buoys 17 and 19) and three stations along the shelf (buoys 50, 52, and 53). The magnitude of diurnal wind fluctuation appeared intermittent in time by a modulation scale of 5–15 days. Diurnal wind variations appeared to be rather coherent in both cross- and along-shelf directions for most measurements. In mid-June, however, there was little evidence of coherence between the cross-shelf components of wind stress at buoys 50, 52, and 53. Good coherence also is seen between the diurnal variations of wind stress and air-sea temperature difference (Figure 14). It is assumed that the surface water was cooled during vertical mixing caused by the diurnal variation in the wind stress magnitudes accompanying frontal passages.

Coherence estimates for hourly wind velocities were made to examine the cross-shelf and along-shelf separation scales of the wind field. The same procedure was used as when estimating coherences for the residual, near-inertial currents. Coherences of wind stress were estimated based on station pairs with different record lengths. To remove bias related to record length, the coherence value of the wind stress at diurnal frequency is plotted relative to its 95% confidence level in Figures 8a and

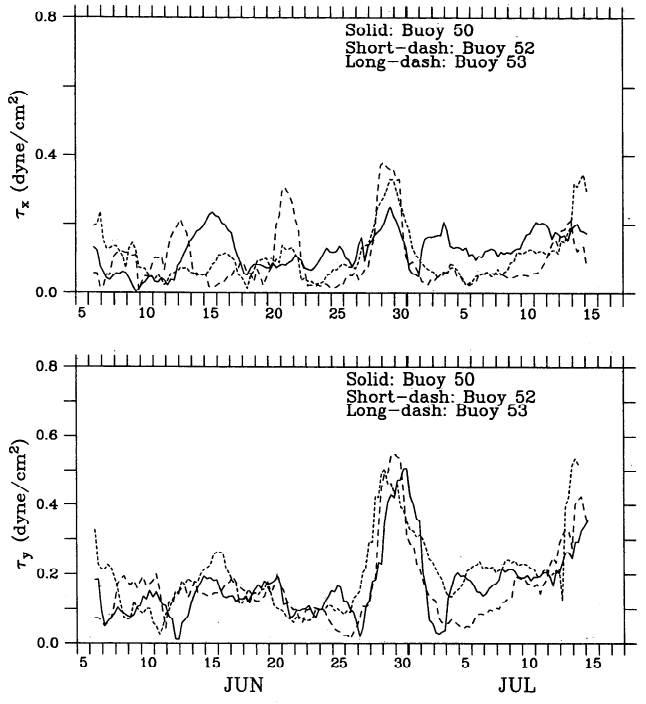

Figure 15. Time series of the eastward (x) and northward (y) components of surface wind stress at diurnal period estimated by complex demodulation of data from LATEX A buoys 50, 52, and 53, located west to east along the inner shelf. A least squares method was used to fit 48-hour segments with a 6-hour overlap.

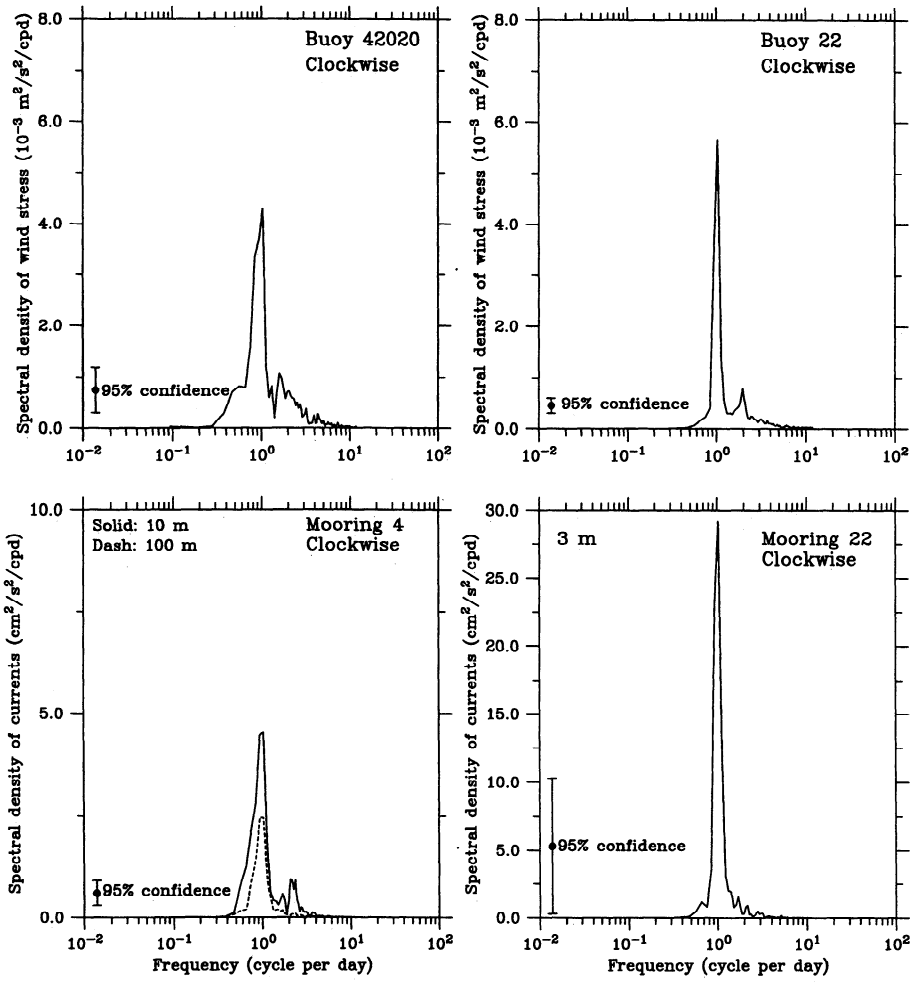

Figure 16. Clockwise-rotating spectra of 40-hour, high-passed wind stress and currents at NDBC meteorological buoy 42020 and mooring 4 from mid-April through May 1992 and at LATEX A meteorological buoy 22 and mooring 22 from early June through August 1992.

8b for all station pairs in the cross-shelf and along-shelf directions. Based on the zero-crossing point relative to the 95% confidence level, Figure 8 shows that the separation scale of diurnal wind variation was about 150 km in the cross-shelf direction and about 350 km in the along-shelf direction.

7. Model Simulation of Near-Inertial Currents by Wind Stress

As described above, the high-frequency oceanic response over the LATEX shelf in the spring and summer of 1992 was mainly dominated by near-inertial motions. These clockwise-rotating currents were characterized by a first-baroclinic mode in the vertical. The energy of the oscillations was surface-intensified, reached its maximum at the shelf break, and decayed gradually onshore and rapidly offshore. The surface intensification implies that wind stress may play the most important role in forcing such oceanic oscillations. Cross-shelf structures of the amplitudes suggest the restriction of the oscillations by a solid boundary at the coast and the variable bottom topography over the continental shelf.

Near-inertial currents were observed in association with the diurnal variation of the wind stress. Examples are shown in Figure 16. At NDBC buoy 42020, the high-frequency wind stress in April and May was dominated by the clockwise-rotating flow with an energetic spectral peak near diurnal frequency. Correspondingly, at nearby mooring 4, the spectra of 40-hour high-passed, residual currents were marked by the near-inertial energy peak at the 10- and 100-m instruments. At current mooring 22 a large inertial energy peak in currents was observed in response to the strong diurnal variation of the wind stress. Evidence for this relationship is visible in time series plots of high-frequency wind stress and water currents demodulated at a 24-hour period (Figures 17 and 18). The relatively strong near-inertial current oscillations kept company with the high-frequency (near-diurnal) variation of wind field during the frontal passage.

Occurrence of the near-diurnal oscillations of the water currents was closely related to the temporal variation of the low-frequency wind field. At mooring 4, for example, the near-inertial oscillations of water currents in the mixed layer generally increased at times when the low-frequency surface wind stress rapidly changed in amplitude and direction during frontal passages (Figure 17). This relation was also evident at inshore mooring 22, where large near-inertial oscillations occurred along with a rapid change of the surface wind stress in mid-June and early August (Figure 18). No significant near-inertial oscillations were observed in the mixed layer after

August 15 at mooring 22 when the wind was counterclockwise-rotating with time during the frontal passage. In this case, the along-shelf and cross-shelf components of input wind forcing canceled each other, so no oscillations would be generated there [*Kundu*, 1986].

Both low- and high-frequency variations of the wind were found coherent with the near-inertial current oscillations, and a quantitative estimate of the wind contribution to the amplitude of current oscillations is sought to understand the dominant mechanism for wind-induced, near-inertial motions. A simple slab-like mixed layer model, driven by the observed surface wind stress, is introduced here to estimate effects of wind forcing. This model is used with the understanding that it is only a first-order approximation for the case when downward transport of near-inertial energy through the mixed layer is small during the oscillations.

Assuming a linear system, the complex governing equation for a slab-like, wind-induced, mixed layer is given by

$$\frac{dU}{dt} + f'U = \tau_s, \tag{1}$$

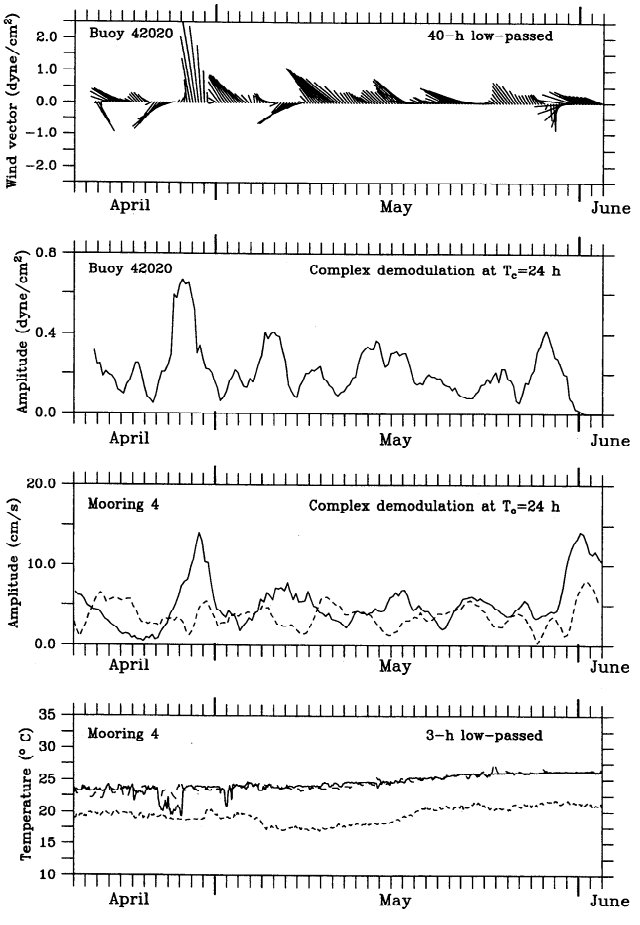

Figure 17. Time series of 40-hour, low-passed wind stick vectors at NDBC meteorological buoy 42020; amplitudes of 40-hour, high-passed wind and currents calculated by complex demodulation at diurnal period at NDBC meteorological buoy 42020 and current mooring 4 (solid line for 10 m; dashed line for 100 m); and 3-hour, low-passed water temperatures at the surface (long-dashed line), 10 m (solid line), and 100 m (short-dashed line).

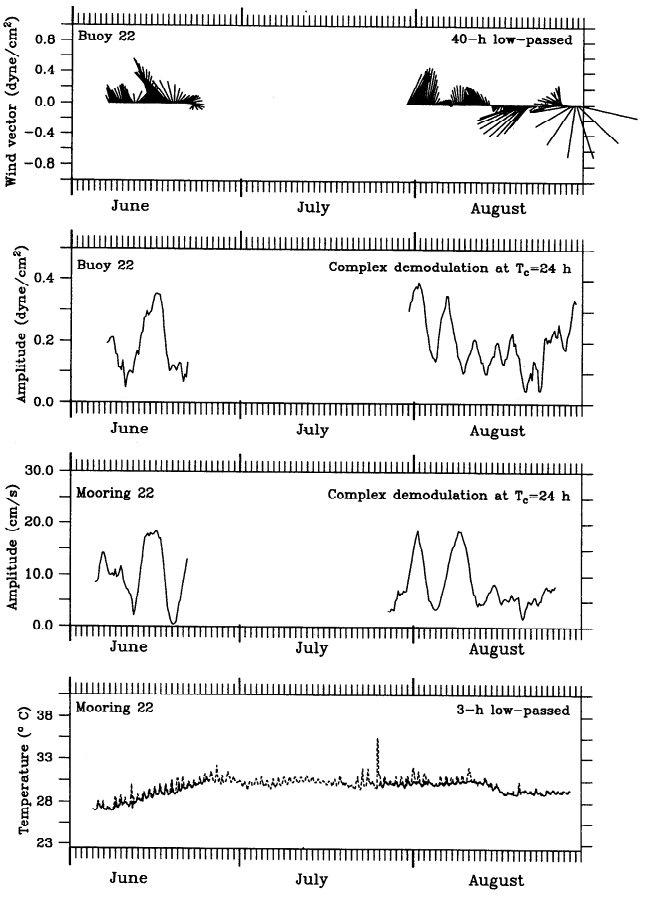

Figure 18. Time series of 40-hour, low-passed wind stick vectors at LATEX A meteorological buoy 22; amplitudes of 40-hour, high-passed wind and 3-m currents calculated by complex demodulation at diurnal period at LATEX A meteorological buoy 22 and current mooring 22; and 40-hour, low-passed water temperatures at the surface (dashed line) and 3 m (solid line).

where $U = hu + ihv$; $\tau_s = (\tau_{sx} + i\tau_{sy})/\rho_0$; $f' = C_0 + if$; u and v are the depth-averaged velocities in the east (x) and north (y) directions; τ_{sx} and τ_{sy} are the x- and y-directed surface wind stresses; h is the thickness of the mixed layer; C_0 is the drag coefficient of internal wave radiation propagating away from the base of the mixed layer; f is the local inertial frequency; and ρ_0 is the density in the mixed layer [*Pollard and Millard*, 1970; *Wood*, 1987]. For this linear case, the complex transport U can be written as the sum of the Ekman transport U_E and the inertial oscillation U_I. Therefore

$$\frac{dU_I}{dt} + f'U_I = -\frac{dU_E}{dt} = -\frac{1}{f'}\frac{d\tau_s}{dt}. \tag{2}$$

The solution of this equation is given by

$$U_I = -\int_0^t \frac{1}{f'}\frac{d\tau_s}{dt} e^{f'(t'-t)}\,dt, \tag{3}$$

where U_I is assumed initially to be zero.

This expression indicates that the surface wind stress must vary with time to produce the inertial oscillations. The theoretical solution is consistent with our observations over the LATEX shelf, which indicate that the near-inertial oscillations

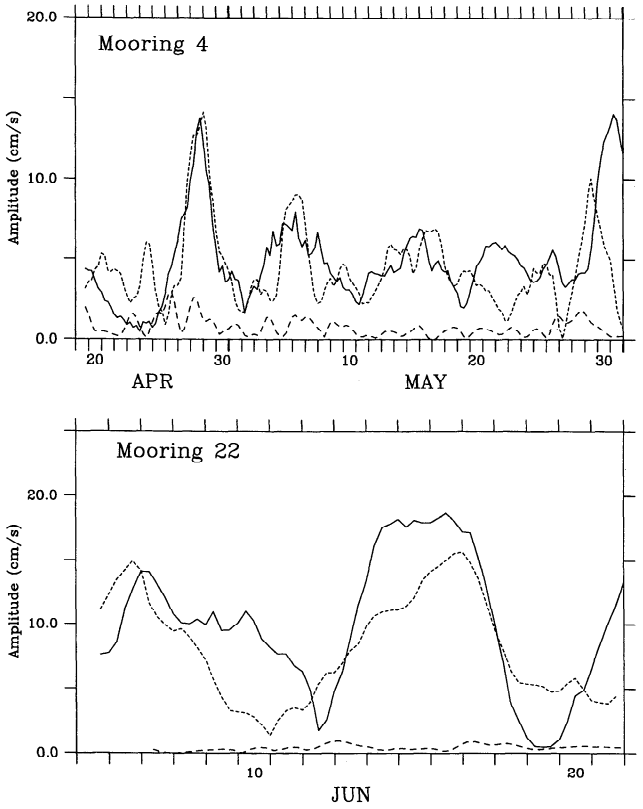

Figure 19. Comparison between amplitudes of observed (solid line) and modeled (short-dashed line) near-inertial currents at 10 m at mooring 4 from April 19 through May 31, 1992, and at 3 m at mooring 22 from June 2 through 21, 1992, using the observed hourly wind forcing. The long-dashed line in each figure indicates the amplitude of the near-inertial currents modeled by 40-hour, low-passed wind forcing.

usually occur when the surface wind changes its direction and speed, as during frontal passages.

Using the observed surface wind stress to force the model, we simulated the near-inertial currents at moorings where a well-defined mixed layer was created by wind mixing during frontal passages. We forced the model by the 40-hour, low-passed and hourly (both low- and high-passed) wind stresses separately and estimated the quantitative contributions of low- and high-frequency wind variations to near-inertial oscillations. Examples are shown in Figure 19 for moorings 4 and 22. The best simulation is obtained with the decay constant of $C_0 = 3.0 \times 10^{-5}\ s^{-1}$ (about 9.2 hours) at these two locations. At mooring 4 the amplitude of the oscillations, predicted by the nearby hourly wind stress at NDBC meteorological buoy 42020, is in reasonable agreement with the observation at 10 m from late April to mid-May. The model also provides a reasonable simulation for the near-inertial currents at 3 m at mooring 22. It is not surprising that the model fails in late May at mooring 4. The observed amplitude of near-inertial oscillations at 100 m is also significant during that time period, implying a large downward transfer of wind-induced energy from the upper mixed layer to the lower stratified layer.

Examples of currents simulated only by low-frequency wind forcing are also shown in Figure 19 for moorings 4 and 22. Although the large near-inertial oscillations usually occurred when the low-frequency wind rapidly changed its direction during the frontal passages, the amplitude of the oscillations generated by the low-frequency winds was negligible. This result suggests that the relatively strong near-inertial oscillations over the LATEX shelf in the spring and summer of 1992 were produced by the high-frequency (near-diurnal) variation of wind field associated with frontal passages.

8. Discussion of Driving Mechanism for Near-Diurnal Variation of the Wind Stress

What causes the strong diurnal wind oscillations over the LATEX shelf? Sea breeze, variation of the air-sea temperature difference, or other mechanisms? Previous coastal meteorological studies have shown that the wind field near the coast is driven by a day-night variation of temperature gradient between the land and sea (so-called sea breeze) [*Hsu*, 1972]). Because daytime air temperatures are high over land and cool over the sea, the air flows toward the land from the sea to compensate for vertical thermal convection over the warmer land. Alternatively, at night the air flows toward the sea from the land because the land cools rapidly. This diurnal variation of cross-shelf temperature gradients causes a diurnal fluctuation of the surface wind field in a range of 1–4 m/s near the Texas coast [*Hsu*, 1972]. Because previous meteorological measurements were limited to a few kilometers from the coast, little information has been reported on the cross-shelf scale of the sea breeze over the LATEX shelf.

Based on the meteorological observations at buoys SRST2

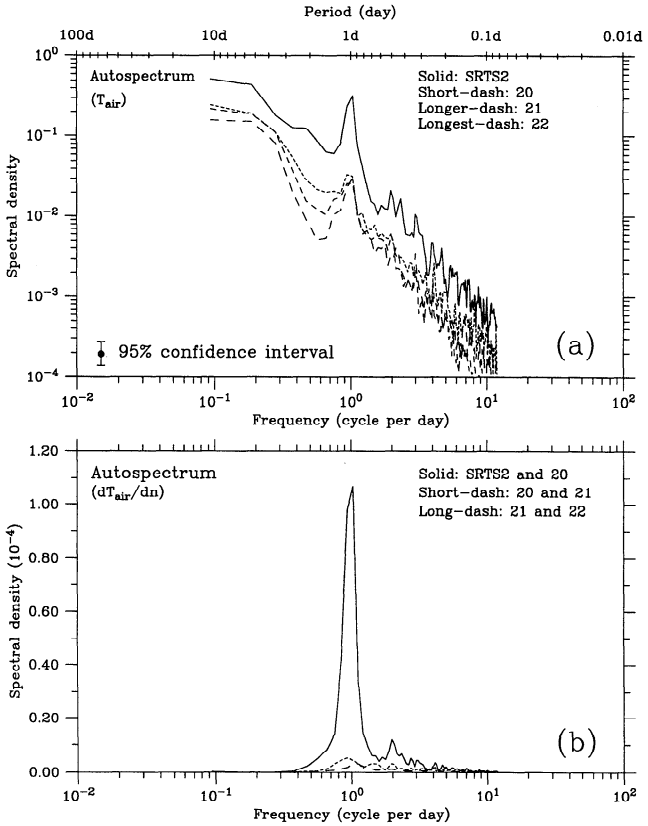

Figure 20. (a) Autospectra for air temperature at SRST2, LATEX A meteorological buoys 20, 22, and 22; (b) 40-hour, high-passed temperature gradients between station pairs: SRST2–buoy 20, buoys 20–21, and buoys 21–22.

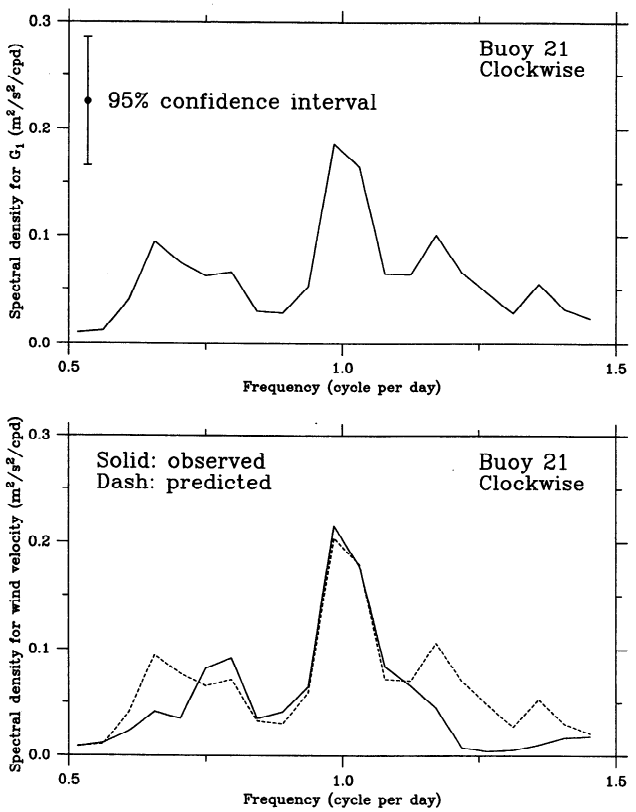

Figure 21. Clockwise components of rotary spectra for the 40-hour, high-passed observed and predicted winds at LATEX A meteorological buoy 21. The estimates were made based on the time series of wind and pressure data taken from April 17 through May 30, 1992, at LATEX A buoys 50, 52, 20, and 22.

and 20–22 in the spring and summer of 1992, a spectral analysis for air temperature was conducted to examine the cross-shelf scale of the sea breeze. Autospectra of air temperatures at each buoy showed a peak at diurnal frequency (Figure 20a). A large difference in magnitude was found only between the coastal station SRST2 and buoy 20, separated by about 50 km. Cross-shelf air temperature gradients were examined for adjacent buoy pairs (Figure 20b). The spectral density of the 40-hour, high-passed, cross-shelf air temperature gradient at diurnal frequency was about 120×10^{-3} $(C/km)^2/cpd$ at station pair SRST2 and buoy 20 but negligible at station pair buoys 20–21 and 21–22. This suggests that the sea breeze was restricted to about 50 km from the coast.

When strong wind stress was imposed at the sea surface over the LATEX shelf during frontal passages, the surface water was cooled due to wind mixing, causing a marked near-diurnal variation of air-sea temperature difference (Figure 14). As a consequence of air-sea interaction, the buoyancy flux associated with sensible heat transport might modify turbulent structures in the marine boundary layer, producing the near-diurnal variation of wind stress. An estimate of the contribution of air-sea temperature difference to the diurnal variation of wind stress was conducted using *Wu*'s [1986] empirical formulae for the wind stress coefficient with correction of the air-sea temperature difference. The formulae are derived for both unstable and stable cases. In the unstable case,

$$C_s/C_{10} = e^{-0.614(\Delta T/U_{10})^{5/3}}$$

and in the stable case,

$$C_s/C_{10} = e^{-0.424(\Delta T/U_{10})^{3/5}}$$

where C_s is the surface wind stress coefficient; C_{10} is the wind stress coefficient at a height of 10 m under neutral conditions; ΔT is the air-sea temperature difference, and U_{10} is the wind velocity at a height of 10 m. On the LATEX shelf, the typical values of U_{10} and ΔT during the frontal passages were about 10 m/s and 0.5°C. Therefore $(C_s/C_{10} - 1)$ was less than 0.01 for both unstable and stable cases. This estimate suggests that the feedback effect of diurnal variation of the air-sea temperature difference on diurnal wind variation was too small to be taken into account over the LATEX shelf in spring and summer of 1992.

We examine here a possible relation between the high-frequency fluctuation of the surface wind and atmospheric pressure gradients, with which we simulate the diurnal wind fluctuation from observed pressure fields. A simple atmospheric boundary layer model is developed here in the form of

$$\frac{\partial W}{\partial t} + if\,(W - G) = \frac{\partial \tau}{\partial z} \tag{4}$$

where $W = w_x + iw_y$; $G = 1/\rho f(-p_y + ip_x)$; $\tau = (\tau_x + i\tau_y)/\rho$; w_x and w_y are the east (x) and north (y) components of the wind velocity; p_x and p_y are the x and y components of the air pressure gradient; τ_x and τ_y are the x and y components of the wind stress; f is the local inertial frequency; and ρ is the air density.

Vertically averaging (4) over the planetary boundary layer h and assuming τ to be zero at top (a level of the gradient wind) gives

$$\frac{\partial \bar{W}}{\partial t} + if\,(\bar{W} - G) = -\frac{\tau_s}{h}, \tag{5}$$

where

$$\bar{W} = \frac{1}{h}\int_0^h W\,dz \tag{6}$$

and G is considered independent of z in the boundary layer.

Separating all variables into a sum of 40-hour, low- and high-passed components such as

$$\bar{W} = W_0 + W_1; \qquad G = G_0 + G_1; \qquad \tau_s = \tau_{s0} + \tau_{s1} \tag{7}$$

where the subscripts "0" and "1" refer to the 40-hour, low- and high-passed signals, respectively, and substituting the variables into (5), we can derive an equation for the high-frequency fluctuation as

$$\frac{\partial W_1}{\partial t} + (\alpha + if)W_1 = ifG_1, \tag{8}$$

where the high-frequency surface wind stress is approximated as

$$\tau_{s1} = h\alpha W_1 \tag{9}$$

with $\alpha = C_d|\bar{W}|/h$ and C_d the drag coefficient. The solution of (8) can be obtained in the form

$$W_1 = if\int_0^t G_1(t')e^{\alpha'(t'-t)}\,dt', \tag{10}$$

where $\alpha' = \alpha + if$ and W_1 is initialized as zero.

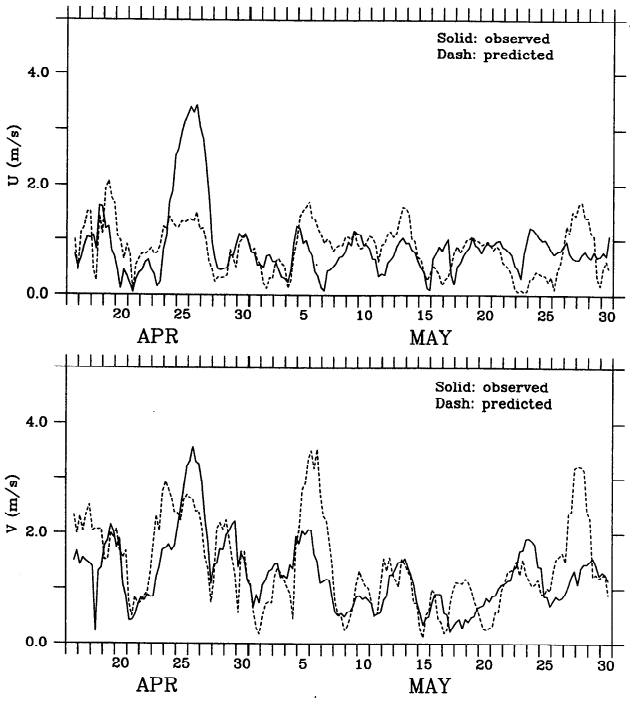

Figure 22. Time series of observed and predicted amplitudes of surface wind components at diurnal period obtained by complex demodulation. Data are from LATEX A meteorological buoy 21 from April 17 through May 30, 1992. A least squares method was used to fit 48-hour segments with a 6-hour overlap.

The prediction of the near-inertial wind from (10) is given next using the observed 40-hour, high-passed air pressure gradients over the shelf. For example, the time series of pressure gradient from mid-April to end of May at meteorological buoy 21 is estimated using the observed pressure data from buoys 20, 22, 50, and 52. The resulting high-frequency pressure gradients show a marked near-diurnal energy peak for the clockwise-rotating motion (Figure 21a). Using this high-frequency pressure gradient in (10), we estimated the inertial wind oscillations at buoy 21. The best solution is found when α equals 0.77×10^{-4} s^{-1}. The predicted wind is in reasonable agreement with the observation in spectral distribution and amplitude (Figures 21b and 22), suggesting that the diurnal variation of the wind stress over the LATEX shelf may be caused by the near-diurnal variation of the high-frequency pressure gradients.

9. Summary

Wind-induced, near-inertial oscillations over the LATEX shelf in spring and summer 1992 are described using the water current and wind observations taken during the first year of the LATEX A program. Rotary spectral analysis showed clockwise-rotating energy peaks at near-inertial frequencies for currents at all current meter moorings. Vertical structures of the near-inertial oscillations were characterized by a first-baroclinic mode with a near 180° phase difference between upper-mixed and lower-stratified layers. The oscillations were intermittent with a modulation time scale of about 5–7 days. They were surface-intensified, had maximum kinetic energy at the shelf break, and decayed gradually toward the coast but rapidly offshore.

In the spring and summer of 1992, the air flow over the LATEX shelf was dominated by southerly winds associated with the subtropic anticyclone. This synoptic-scale wind field was intermittently altered with the passage of fronts associated with low-pressure cells. Rotary spectra showed marked clockwise-rotating energy peaks near-diurnal frequency for all meteorological buoys over the shelf. The large near-diurnal variation of the wind stress kept company with the frontal passages. Sea breeze was found significant only to a cross-shelf distance of 50 km from the coast. The feedback effect of diurnal variation of the air-sea temperature difference on the near-diurnal wind variation was too small to be taken into account. Results of a simple atmospheric boundary model suggest that the near-diurnal variation of wind stress possibly is related to the diurnal variation of the atmospheric pressure gradients.

The cross- and along-shelf coherence scales of the diurnal wind stress were about 150 km and 350 km, respectively. The coherence scale of the near-inertial currents was about 300–350 km in the along-shelf direction but only 80 km in the cross-shelf direction. Near-inertial oscillations appeared to accompany the variation of the wind stress during frontal passages. Diagnostic analysis suggests that large near-inertial oscillations over the LATEX shelf were mainly generated by the high-frequency (near-inertial) variation of the wind stress associated with the passage of atmospheric fronts. When the downward transfer of the near-inertial energy to the deep stratified layer was small, a simple mixed layer model forced by the observed wind stress provided a reasonable prediction of the near-inertial currents in the mixed layer.

Acknowledgments. This research was supported by the Minerals Management Service, U.S. Department of the Interior, under OCS contract 14-35-0001-30509. We would like to thank Linwood Lee, Frank Kelly, and Matthew Howard in the LATEX A Data Office for their efforts in quality control of the data. Also, we want to thank Bob Beardsley and Dave Chapman at Woods Hole Oceanographic Institution for their valuable comments and suggestions.

References

Barron, C. N., Jr., and A. C. Vastano, Satellite observations of surface circulation in the northwestern Gulf of Mexico during March and April 1989, *Cont. Shelf Res.*, *14*, 607–627, 1994.

Beardsley, R. C., C. E. Dorman, C. A. Friehe, L. K. Rosenfeld, and C. D. Winant, Local atmospheric forcing during the coastal ocean dynamics experiment, 1, A description of the marine boundary layer and atmospheric conditions over a northern California upwelling region, *J. Geophys. Res.*, *92*, 1467–1488, 1987.

Brooks, D., The wake of Hurricane Allen in the western Gulf of Mexico, *J. Phys. Oceanogr.*, *13*, 117–129, 1983.

Clarke, A. J., The dynamics of barotropic tides over the continental shelf and slope (review), *Tidal Hydrodynamics*, edited by B. B. Parker, pp. 79–108, John Wiley, New York, 1991.

Clarke, A. J., and K. H. Brink, The response of stratified, frictional flow of the shelf and slope waters to fluctuating large-scale, low-frequency wind forcing, *J. Phys. Oceanogr.*, *15*, 439–453, 1985.

Denbo, D. W., and J. S. Allen, Rotary empirical orthogonal function analysis of currents near the Oregon coast, *J. Phys. Oceanogr.*, *14*, 35–46, 1984.

Ekman, V. W., On the influence of the Earth's rotation on ocean currents, *Ark. Mat. Astron. Fys.*, *2*, 1–52, 1905.

Foreman, M. G. G., Manual for tidal currents analysis and prediction, *Pac. Mar. Sci. Rep. 78–6*, 70 pp., Inst. of Ocean Sci., Patricia Bay, Sidney, B. C., Canada, 1979.

Fu, L. L., Observations and models of inertial waves in the deep ocean, *Rev. Geophys.*, *19*, 141–170, 1981.

Gill, A. E., *Atmospheric-Ocean Dynamics*, 662 pp., Academic, San Diego, Calif., 1982.

Gill, A. E., On the behavior of internal waves in the wakes of storms, *J. Phys. Oceanogr.*, *14*, 1129–1511, 1984.

Gonella, J., A rotary-component method for analyzing meteorological and oceanographic vector time series, *Deep Sea Res.*, *19*, 833–846, 1972.

Hendershott, M. C., Inertial oscillations of tidal period, *Prog. Oceanogr.*, *6*, 1–27, 1973.

Hsu, S. A., Coastal air-circulation system: Observations and empirical model, *Mon. Weather Rev.*, *98*, 487–509, 1972.

Kroll, J., The propagation of wind-generated inertial oscillations from the surface into the deep ocean, *J. Mar. Res.*, *33*, 15–51, 1975.

Kundu, P. K., A two-dimensional model of inertial oscillations generated by a propagating wind field, *J. Phys. Oceanogr.*, *16*, 1076–1084, 1986.

Kundu, P. K., and R. E. Thompson, Inertial oscillations due to a moving front, *J. Phys. Oceanogr.*, *15*, 1076–1084, 1985.

Large, W. S., and S. Pond, Open ocean momentum flux measurements in moderate to strong winds, *J. Phys. Oceanogr.*, *11*, 324–406, 1981.

Millot, C., and M. Crepon, Inertial oscillations on the continental shelf of the Gulf of Lions: Observations and theory, *J. Phys. Oceanogr.*, *11*, 639–657, 1981.

Mooers, C. N. K., A technique for the cross spectrum analysis of pairs of complex-valued time series, with emphasis on properties of polarized components and rotational invariants, *Deep Sea Res.*, *20*, 1129–1141, 1973.

Munk, W., and N. Phillips, Coherence and band structure of inertial motion in the sea, *Rev. Geophys.*, *6*, 447–472, 1968.

Nowlin, W. D., Jr., J. S. Bottero, and R. D. Pillsbury, Observations of internal and near-inertial oscillations at Drake Passage, *J. Phys. Oceanogr.*, *16*, 87–108, 1986.

Pollard, R. T., On the generation by winds of inertial waves in the ocean, *Deep Sea Res.*, *17*, 795–812, 1970.

Pollard, R. T., and R. C. Millard, Comparison between observed and simulated wind-generated inertial oscillations, *Deep Sea Res.*, *17*, 813–821, 1970.

Price, J. F., Internal wave wake of a moving storm, I, Scales, energy budget, and observations, *J. Phys. Oceanogr.*, *13*, 949–965, 1983.

Reid, R. O., and R. E. Whitaker, Numerical model for astronomical tides in the Gulf of Mexico: Theory and application, technical report, 115 pp., Dep. of Oceanogr., Tex. A & M Univ., College Station, 1981.

Vastano, A. C., and C. N. Barron Jr., Comparison of satellite and drifter surface flow estimates in the northwestern Gulf of Mexico, *Cont. Shelf Res.*, *14*, 589–605, 1994.

Webster, F., Observations of inertial-period motions in the deep-sea, *Rev. Geophys.*, *6*, 473–490, 1968.

Wood, T. M., Observations of inertial oscillation during the Nantucket Shoal flux experiment, M. S. thesis, 112 pp., MIT/WHOI Joint Program, Cambridge, Mass., 1987.

Wu, J., Stability parameters and wind-stress coefficients under various atmospheric conditions, *J. Phys. Oceanogr.*, *3*, 333–339, 1986.

C. Chen, Department of Marine Sciences, University of Georgia, Ecology Building, Athens, GA 30602-2206. (e-mail: chen@whale.marsci.uga.edu)

W. D. Nowlin Jr. and R. O. Reid, Department of Oceanography, Texas A&M University, College Station, TX 77843.

(Received September 14, 1994; revised August 21, 1995; accepted September 6, 1995.)